Development of Discrete Nanopores I: Tension of Polypropylene/ Polyethylene Copolymer Blends

Jonghwi Lee,* Christopher W. Macosko, Frank S. Bates

Chemical Engineering and Materials Science, The University of Minnesota, Minneapolis, MN 55455

Received 29 July 2003; accepted 17 September 2003

ABSTRACT: Porous polymeric materials can be prepared by using micromechanical deformations. The development of porous structures in the tension of polyolefin blends are studied with the goal of developing a novel technique to make porous films. It is found in polypropylene/polyethylene copolymer blends of near 50/50 weight ratio that a metallocene polymer pair can produce stable nanopores throughout a wide range of strain, ~50–700%. Its strain-to-break was relatively high, although its continuous phase is a brittle polypropylene. The typical size of nanopores is 10–300 nm; they start to develop at approximately 50% strain. The disruption of craze-like structures into discrete nanopores seems to be the key mechanism in stabilizing pore development. Varying stretching direction and speed controls the pore morphology. © 2004 Wiley Periodicals, Inc. J Appl Polym Sci 91: 3642–3650, 2004

Key words: polyolefins; crazing; poly(propylene) (PP); polyethylene copolymers; porous film

INTRODUCTION

Porous polymers are used in a wide range of industries from electronics to bioengineering.[1–6] Typical porous polymeric materials are produced by various techniques, such as stretching of filled polymers, phase separation, supersaturating of gas, leaching, or deposition. Specifically, the stretching method, which is simple, cheap, and environmentally safe, is utilized in the breathable film industry usually using $CaCO_3$ particles embedded in polyolefins.[6] Inorganic particles in the polyolefin matrix act as stress concentrators initiating annular microcracking. The microcracks further develop into pores via yielding of the matrix. Typical pore size generated by this process ranges from 0.1 to 1 μm, which can selectively prevent liquid water leaking and allow water vapor transport through polyolefin films.[6] These films are used for diapers, medical devices, membranes, filters, roofing, artificial paper, and household wrap.[6]

This cost-effective and fast process of producing porous film has several disadvantages. First, precise control over pore size and its distribution is not readily achievable.[6] Both dispersing small (2–3 μm) inorganic particles in polymers[7] and subsequent stable pore development around them are important but difficult to regulate. Second, the use of inorganic particles can produce serious wear problems in manufacture processing lines. Third, the incorporation of inorganic particles into polymers also limits the physical properties of final products such as texture and color.

Instead of inorganic particles, an immiscible polymer can be introduced into the polyolefin matrix. By varying the interfacial strength between the two polymers, the stress concentration at interface can be controlled, which leads it to control the morphology of the polymer phases. This way of tailoring the stress concentration at the polymer blend interface is expected to bring effective control over the development of porous structures. Moreover, different types of polymers show quite different development mechanisms of pores. Thus, it is possible that, by selecting different polymers, a wide range of porous structures can result.

Among various polymers available for replacing $CaCO_3$ in polyolefin matrices, a polyolefin different from the matrix polyolefin is an excellent candidate, because interfacial strength between two polyolefins can vary over a wide range.[8–13] Recently, the use of metallocene catalysts dramatically improves the regularity in the stereochemistry of polyolefins, while reducing side reactions that cause the random branching of the polymer.[14] Polyolefins are also attractive candidates for replacing $CaCO_3$ from an industrial point of view. As generally known, having fast-growing application areas, polyolefins are the most widely used cheap plastic materials.[15,16]

In this study, our objective was to examine the kinds of porous structures that develop and how they develop in polymer blends under a tensile load. Blends

Correspondence to: J. Lee (jlee@sejong.ac.kr).

*Current address: Department of Nano Science and Engineering, Sejong University, Kwang-Jin-Gu, Gun-Ja-Dong 98, Seoul, Korea (South).

Journal of Applied Polymer Science, Vol. 91, 3642–3650 (2004)

TABLE I
Designations and Physical Properties of Polymers

Designations	PE-m1	PE-m2	PP-m	PP-z
Trade Name	EXACT 4033	EXACT 0201	ACHIEVE PP3825	ESCORENE PP4062
M_w (kg/mol)	118	78	27	48
Polydispersity	2.1	2.1	2.0	2.4
Catalyst	Metallocene	Metallocene	Metallocene	Ziegler-Natta
Comonomer	Butene (11.4 mol %)	Octene (4.6 mol %)	—	—
Density (g/cc)	0.880	0.902	0.900	0.900
Melt flow rates (g/10 min)	0.8	1.1	32	3.6
T_m[a] (°C)	63 (50)	96 (82)	150 (111)	163 (113)
Crystallinity[b] (%)	5	35	35	40

[a] T_m is melting temperature measured by differential scanning calorimeter (DSC). T_c is recrystallization temperature on cooling from 200°C at −10°C/min and is reported in parentheses. Samples were annealed at 200°C for 2 min before recrystallization.
[b] Calculated from DSC data.[38]
Note: All data except T_m, T_c, and crystallinity were provided from the manufacturer.

of two metallocene polyethylene copolymers (PE), one Ziegler-Natta, and one metallocene polypropylene (PP) were used to prepare PP/PE films of 60/40, 40/60, and 50/50 weight ratios. Special attention was placed on the effects of crazing leading to the development of pore structures within the film.

Understanding the initiation and growth of pores in polyolefin blends is fundamental knowledge for developing and engineering the materials. However, the mechanical responses of semicrystalline polymers are generally more complicated to understand and predict than those of amorphous polymers.[17] This is mainly due to the coexistence of amorphous and crystalline phases. If two different semicrystalline polymers are mixed, more complicated mechanical responses are expected. The aim of this study was to lead us to better understand this class of materials.

EXPERIMENTAL

Materials

Two PEs, Exact 4033 and Exact 0201, were provided by ExxonMobil. Since Exact 4033 has a higher comonomer content (11.4 mol %), its modulus was found to be lower than Exact 0201. Additionally, two PP homopolymers were provided by ExxonMobil, Achieve PP3825 and Escorene PP4062. The designations and physical properties of polymers can be found in Table I.

Preparation of polyolefin films

Before melt blending, polymer pellets were dried under vacuum at room temperature for 5 days. Mechanically mixed polymer pellets of 25 g were then melt-blended in a Haake Rheomix 600 at 190°C and 50 rpm (maximum shear rate = 65 s^{-1}) for 5 min and then quenched in liquid nitrogen. After drying under vacuum for 3 days, the blends were hot-pressed into films of ~100 μm thickness for 5 min at 190°C under 1 metric ton. A stainless-steel spacer of 277 (±5) μm thickness and poly(ethylene terephthalate) film covers were used. The polyolefin films were characterized after 3 days of physical aging at room temperature.

Characterizations

For tensile tests, five rectangular films of 8 × 18 × 0.1 mm were prepared and loaded in a MTS MicroBionix instrument with a 4*N* load cell (span = 10 mm) at room temperature (displacement rate = 8 mm/min). The dimensions of the specimens were measured using a micrometer, NSK digitrix II (resolution = ±1 μm). Displacement measured by the MTS instrument was calibrated using the digital images of two points on a specimen under stretching. A CCD camera, Sony SSC-M370 with NAVITAR TenX lens, was used to capture the images of the stretched specimens. For PP homopolymers, five dog-bone–shaped specimens (gauge section = 0.1 × 4 × 20 mm) were prepared and tested in addition to the rectangular specimens (displacement rate = 14 mm/min). No significant differences were found in the tensile test results of the two types of specimens. Thus, specimen geometry does not seem to be critical in this experiment, although the PP homopolymers showed brittle fracture at relatively small strain (<1). The Young's moduli of the polymer films were obtained from the initial linear parts of stress–strain curves (usually 0–0.2% strain).

Transmission electron microscopy (TEM) micrographs were obtained by first imbedding each polyolefin film in an epoxy resin (Tra-Con BA-2115), followed by a curing step at room temperature for more than 24 h. The specimens were then microtomed at –120°C using a glass knife and stained by RuO_4 for

6–24 h.[18–21] Thin sections of 70–80 nm thickness were cut by a Microstar diamond knife, and examined using a Jeol 1210 electron microscope at an accelerating voltage of 120 kV.

Scanning electron microscopy (SEM) samples, coated with 5 nm Pt-Pd, were examined using a field emission-gun Hitachi S-800 microscope at 3–5 kV. The microscope was operated at 3 kV to prevent electron beam damage, when its magnification is higher than 10 k.

A differential scanning calorimeter (DSC), Perkin–Elmer Pyris 1, was used to measure the melting point and crystallinity of the polymer films between $T = -150 \sim 200°C$ at a heating rate of 10°C/min (Table I). The mass of the homopolymers used in the DSC was 5 mg, while the mass of the blend samples was 10 mg.

RESULTS

Basic physical properties of polymers

The physical properties of homopolymers and their blends are given in Table I, which shows that PE-m1 has 11.4 mol % butene units, while PE-m2 has 4.6 mol % octene units. The incorporation of both comonomers considerably decreases the melting temperature (T_m), and makes polyolefins more rubbery. The T_m data in Table I lead us to speculate that PE-m1 is generally softer than PE-m2. In fact, this is true and can be noticed by handling these two polymer films; it can also be confirmed in their stress–strain curves, which will be discussed later. The density and crystallinity data of Table I are also consistent with PE-m1 being softer than PE-m2.

PP-m is prepared by a metallocene catalyst, and, in contrast, PP-z is made from a conventional Ziegler-Natta catalyst. PP-z has only a slightly higher polydispersity than PP-m. While polydispersity is not considerably varied, it was reported that the Ziegler-Natta–prepared polyolefin, PP-z, has a substantial amount of noncrystallizable chains.[8,10,22] In PP-z, molecular weight is higher and melt flow rate is lower. Thus, when PP-z and PP-m are mixed with a PE, phase inversion is likely to occur at different compositions.[23]

Uniaxial tensile tests

Figure 1 shows the uniaxial tensile test results of the polymer films prepared by hot pressing, which generally produces weaker films than injection molding. Here, PP polymers undergo brittle failure. This behavior is observed during the stretching of PP, where it develops localized stress whitening (necking) in a small region (usually less than 2 mm), followed by the abrupt failure of the region. In the brittle failure of PP, crazing (or at least craze-like deformation) is thought

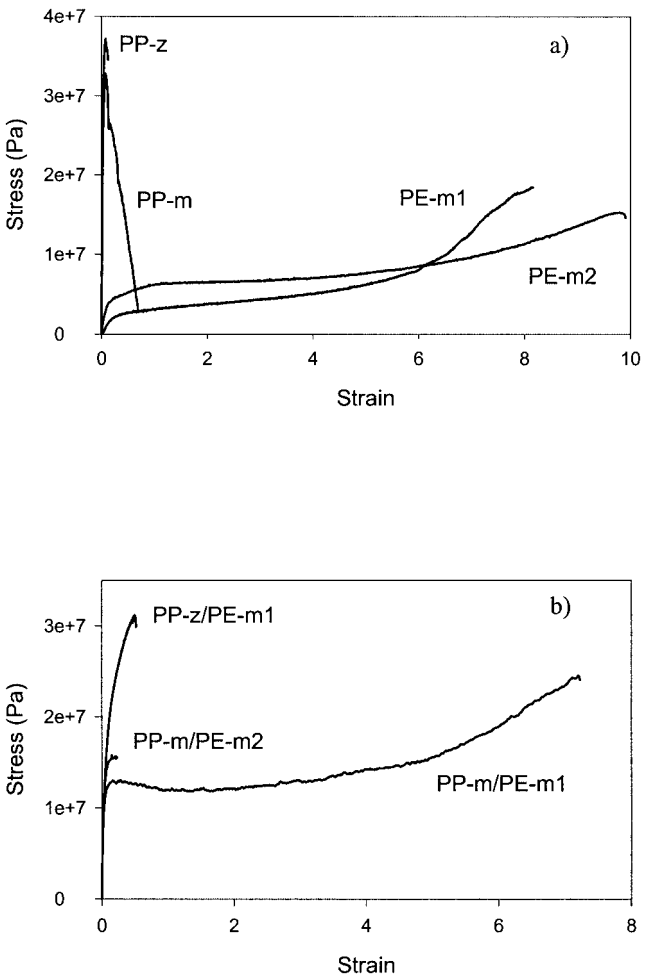

Figure 1 Typical uniaxial tensile behavior of polypropylene/polyethylene copolymer blends at a displacement of 8 mm/min: (a) homopolymers; (b) 50/50 blends.

to play a major role. Typical craze (or craze-like) structures (CS) in semicrystalline polymers are not as regular as in amorphous polymers such as polystyrene and polycarbonate.[24–27]

In contrast to PP, PE polymers deform in ductile modes similar to rubber. Figure 1(a) shows that PE polymers undergo a uniform yielding over a wide range. This yielding is followed by strain hardening and failure. The strain-to-break of the PE films[8–10] is much higher than PP films (<1). It was noted that the PE films remained transparent as they were stretched and stress whitening was not observed. Comparisons between the two polyethylene copolymers show that PE-m1 has a lower modulus and yield stress than PE-m2. However, because of more significant strain hardening, PE-m1 shows a higher stress-to-break.

The tensile behavior of pure polyolefins discussed above is essential to understand that of 50/50 blends. The stress–strain curves of 50/50 PP/PE blends [Fig. 1(b)] show a distinct difference between PP-m/PE-m1 and the others. The strain-to-break of PP-m/PE-m1 is

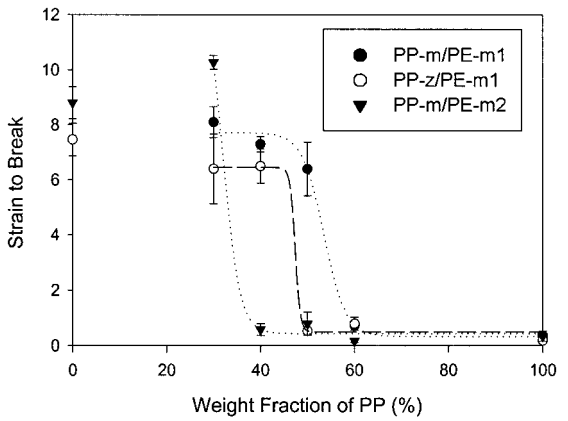

Figure 2 Uniaxial tensile test data: strain-to-break of polyolefin blends as a function of composition at a displacement of 8 mm/min. The plotted lines are guides to the eye.

remarkably higher than those of PP-z/PE-m1 and PP-m/PE-m2, where all five specimens of PP-m/PE-m1 could sustain above a 400% strain upon uniaxial tension, while all the other specimens failed. Thus, the random incorporation of critical defects cannot be the cause for the difference in the stress–strain behavior of the blends. A possible cause of the strain-to-break behavior may be the cocontinuous structure[23] of the 50/50 blends, if it exists. The difference found in strain-to-break is discussed below. Strain-to-break is a critical parameter when we need to use micromechanical deformation phenomena for processing of porous materials, because it will determine the processing window.

Macroscopic observation on the tensile specimens of the 50/50 blends under tension revealed that stress-whitened regions developed in all the specimens before fracture. However, PP-m/PE-m1 had nonlocalized stress whitening and shear yielding, but PP-m/PE-m2 and PP-z/PE-m1 underwent localized stress whitening (necking), immediately followed by fracture. The sources of the stress whitening, such as microcracking, CS, or void formation are expected to exist in the whole specimens of PP-m/PE-m1. This expectation was confirmed by electron microscopy studies.

Figure 2 shows the strain-to-break data as a function of composition. In all three of the blends, there is a distinct transition in strain-to-break, regardless of the blend: as the content of PP decreases, strain-to-break undergoes a step increase (i.e., brittle-to-ductile transition) at ~30–60 wt % of PP. This step transition is expected, since PE will replace PP continuous phase with an increase in PE content.

Electron microscopy study 1: Morphology of blends

The tensile behavior of the polymer blends can be understood based on an electron microscopy investigation of micromechanical deformations. Before the deformations are discussed, the morphology of blends before stretching needs to be identified. The morphology of blends was examined by both TEM and SEM using the RuO_4 heavy staining technique[18–21] to obtain proper contrast between the two phases. PE copolymers were more stained by RuO_4 than PP, resulting in darker phase images in TEM micrographs and brighter images in SEM micrographs.[20,21] Figure 3 shows the TEM micrographs of cross sections of the 50/50 blends. The dark droplets of PE phase can be found in the 50/50 blends of PP-m/PE-m1 and PP-m/PE-m2. The size of PE droplets was polydisperse, and they were generally larger in PP-m/PE-m2. In both cases, the PP forms continuous phase (matrix). On the other hand, PP-z/PE-m1 (50/50) shows rather cocontinuous structures.[23] It seems to be near its phase inversion point. Figure 3(d) shows elongated PE phase images in a broken tensile specimen. Their aspect ratio reflects the strain-to-break of PP-m/PE-m1.

Theoretical prediction of phase inversion points based on the melt flow rate data in Table I may be possible, but it is not always reliable.[23] Thus, an approximation of the phase inversion points for specimens of the three compositions (40/60, 50/50, and 60/40) were assessed from further TEM and SEM

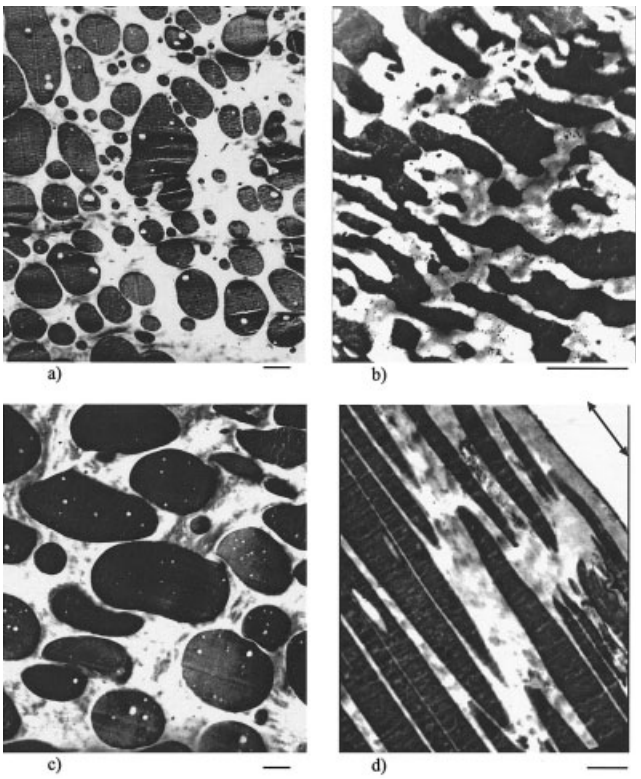

Figure 3 TEM micrographs of the morphology of 50/50 blends: (a) PP-m/PE-m1; (b) PP-z/PE-m1, (c) PP-m/PE-m2, (d) PP-m/PE-m1. The micrographs a, b, and c were taken before tensile tests and d was after tensile tests. The scale bar is 2 μm. (PE phase is dark; PP is light.)

examinations. At least three specimens of each composition were examined. This microscopy investigation showed that both PP-m/PE-m1 and PP-m/PP-m2 had phase inversion between 40 and 50 wt % of PP, and PP-z/PE-m1 near 50 wt % of PP. The same result can also be obtained from the observation made in Figures 3(a—c). PE phase forms droplets in all PP-m/PE-m1 and PP-m/PP-m2 50/50 blends, but not in PP-z/PE-m1 (50/50). On the other hand, each blend shows its step increase at a different PP content (~35, 45, and 55 wt % for PP-m/PE-m2, PP-z/PE-m1, and PP-m/PE-m1, respectively) in Figure 2. Thus, a step increase does not always occur at the phase inversion composition. Although phase inversion can be a cause of step transition, it cannot fully explain the results of Figure 2, particularly where a step increase in strain-to-break occurs.

Interestingly, the PP-m/PE-m1 (50/50) blend has the largest strain-to-break, but has a PP continuous phase instead of a PE matrix. Although the PP phase has continuity in PP-m/PE-m1 blend films, the brittle micromechanical deformations of PP did not develop into macroscopic failure, when strain is less than 700%. Thus, there must be distinct differences in the micromechanical deformations between the PP-m polymers in PP-m/PE-m1 (50/50) and the PP-m homopolymer. The TEM micrograph of a fractured specimen of PP-m/PE-m1 (50/50) in Figure 3(d) clearly shows significant yielding:[28] PE phases are considerably elongated to the direction of the far-field tensile stress.

Electron microscopy study 2. SEM microscopy

During the stretching of PP-m/PE-m1 (50/50) blend films, various micro- and nanoporous structures were found to develop on the surface (plane stress condition) and inside the specimen.[29–32] Figure 4 shows the evolution of surface porous structures with an increase in strain. Since these micrographs were taken after removing the far-field stress, permanent damages were thought to remain. When the strain is about 0.4–0.6, CS starts to develop as band structures, whose direction is perpendicular to the tensile stress. The band structures in Figure 4(a) look similar to typical mature crazes.[24] The internal structure has pores and fibrils.

As strain increases from 0.6 to 2.0, the band structures become disrupted, probably due to significant shear yielding in both phases. After disruption of band structures, discrete nanopores can be found almost everywhere on the film surface. In the high magnification SEM micrograph of Figure 4(b), surface features suggest that materials have been substantially drawn to the tensile stress direction. This is supported by the discrete pores being aligned in the tensile stress direction. Further, these pores are rather irregular, not perfectly circular. They were predominantly found in PP-m/PE-m1 films, not in the PP-z/PE-m1 and PP-m/PE-m2 blends.

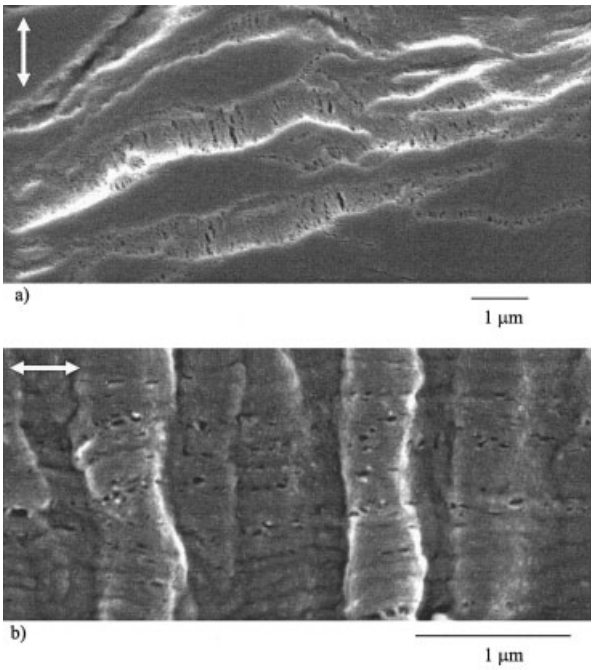

Figure 4 SEM micrographs of surface craze-like structures of PP-m/PE-m1 (50/50) blend: (a) $\epsilon = 0.6$; (b) $\epsilon = 7$. The arrows indicate the direction of far-field stress.

Electron microscopy study 3. TEM microscopy

The disruption of the CS could be found beneath the film surface. Figure 5(a) shows a group of pores that resulted from the disruption of a band structure. The pores are likely to exist initially as a CS band perpendicular to the direction of far-field stress. As strain increases, they become separated and distributed along the interface, parallel to the direction of far-field stress. It should be noted that the direction of interface becomes similar to that of far-field stress with the increase of the strain [Fig. 3(d)].

Figures 5(b and c) show CS in a broken specimen of PP-z/PE-m1 (60/40). This micrograph is typical of the band structures found in the broken specimens of PP-m/PE-m2 and PP-z/PE-m1 60/40, 50/50, and 40/60 compositions. Similar but much smaller structures were also found in PP-m/PE-m1 specimens when strain is lower than 100%. The magnified image of Figure 5(c) shows the fibril-like structures of CS. The CS seems to develop from the interface between PP and PE phases and then spans the whole PP phase. Because of stress concentration at interface, it is anticipated that CS formation starts from the interfacial regions. If the CS in Figure 5(b) continually develops, the load-carrying capability of the PP phase will be

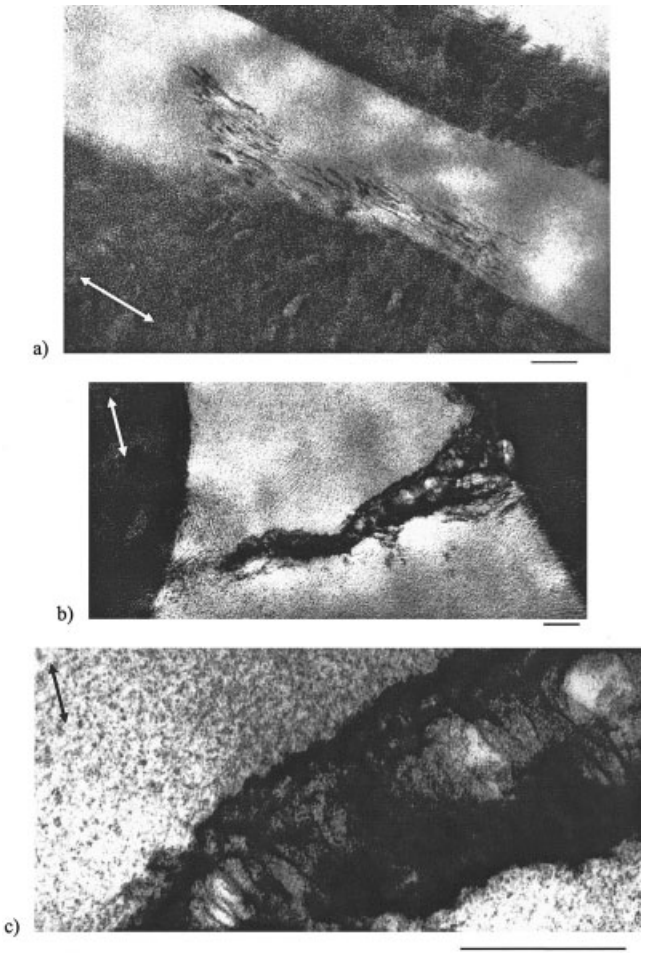

Figure 5 TEM micrographs of craze-like structures developed under uniaxial tension: (a) PP-m/PE-m1 (50/50); (b) PP-z/PE-m1 (60/40); (c) magnified image of the same craze-like structures in b. The scale bar is 100 nm. The arrows indicate the direction of far-field stress. (PE phase is dark; PP is light.)

considerably dampened. These series of events were observed in PP-z/PE-m1 and PP-m/PE-m2, but not in PP-m/PE-m1.

The micromechanical deformation of CS depends on local stress conditions. The strength of interface is a determining factor of local stress concentration in addition to the modulus and strength of each phase. Thus, the interfaces between PP and PE phases were investigated in TEM and typical micrographs are shown in Figure 6. Lamellae that cross the interfaces were found in the unstretched 50/50 blends. They were consistently visible in all specimens both before and after stretching. The lamellae can strengthen the interface by mechanical interlocking.[11,33] The existence of lamellae across the interface indicates possible induced crystallization[34] or differences in crystal structure at the interfacial regions. These events can be followed by different crazing behavior, depending on the crystal structures that result from induced crystallization.[33–35] Although quantitative comparisons cannot be made from the microscopy results, the three blends appear to be strongly adhered at their interfaces. In our recent adhesion experiments, PP-m/PE-m2 displayed the highest interfacial strength among the three blend systems.

Two-step biaxial tension

The development of porous structures during tension could depend on various experimental parameters, such as film processing and stretching parameters. By changing the parameters, the growth of pores can be adjusted too.[36,37] In Figure 7, uniaxially stretched and multiaxially stretched films are compared. They were deformed only until $\epsilon = 4.0$. The multiaxial stretching was performed stepwise. First, a film was initially stretched and unloaded in uniaxial tension [Fig. 7(i)]. It then was stretched in the direction perpendicular to the initial tensile direction [Fig. 7(ii)]. After the initial tension, a much lower yield stress is found in the second step stretching [Fig. 7(ii)]. On the other hand, if the film stretched in the first step is stretched further

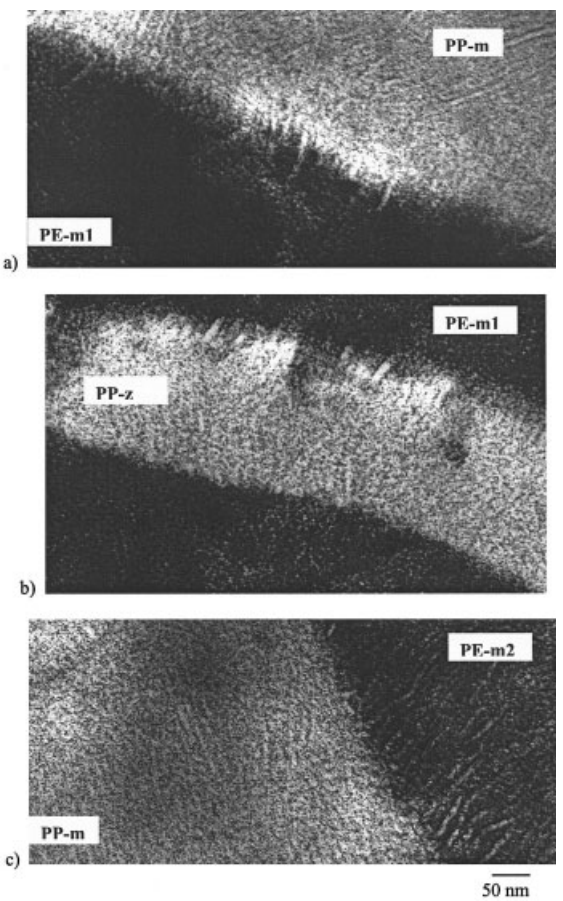

Figure 6 TEM micrographs of the interfacial regions of polyolefin blends (50/50): (a) PP-m/PE-m1; (b) PP-z/PE-m1; (c) PP-m/PE-m2.

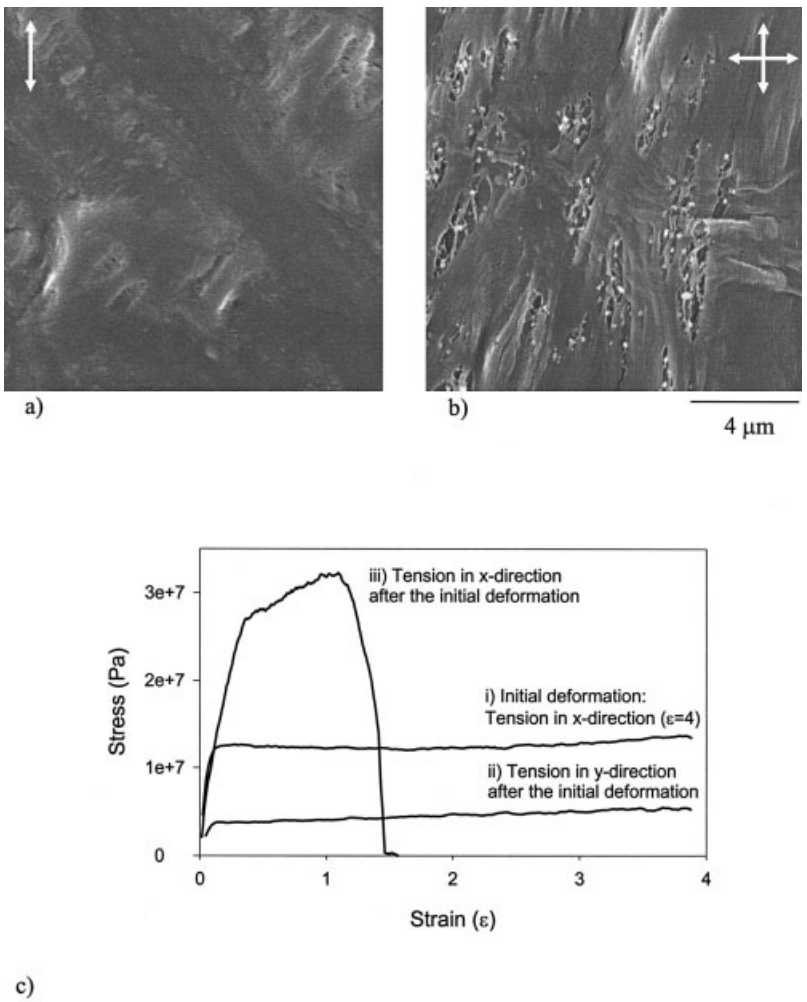

Figure 7 Effect of two-step stretching on the surface pores of PP-m/PE-m1 (50/50): (a) uniaxial, SEM micrographs after tension of $\epsilon = 4$ in x-direction (c, i); b) biaxial, SEM micrographs after tension of $\epsilon = 4$ in y-direction, which was applied after the tension of a (c, ii); (c) typical stress–strain curves. The arrows indicate the direction of far-field stress.

in the same direction [Fig. 7(iii)], a much higher yield stress can be observed, followed by failure at a low strain < 2. Figure 7(a) shows the surface of a uniaxially stretched film, where microcracks are not quite distinct. On the other hand, the two-step multiaxial stretching produces more distinct surface cracks [Fig. 7(b)], which seem to result from the opening of sharp cracks developed in the first step. In our studies, an increase in displacement rate was also found to be effective for controlling pore morphology. By increasing displacement rate from 8 to 80,000 mm/min, distinct differences in surface features could be obtained.

DISCUSSION

The extent of stretching is an important parameter for the possible future development of porous materials processing. Among the three 50/50 blends, PP-m/PE-m1 has the highest strain-to-break value. Macroscopic observation shows that PP-m/PE-m1 (50/50) undergoes significant yielding (Fig. 1) and brittle-to-ductile transition at a lower PE content than the other blend systems (Fig. 2). Microscopic observation reveals the existence of disrupted crazes (discrete nanopores) in the PP phase. Since they partially retain the CS, they are believed to originate from CS. Thus, the initiation of CS and the following disruption process with stretching seem to produce the discrete nanopores. This process explains the reason why the initiation of CS does not lead to macroscopic brittle failure through craze growth. The disruption stabilizes CS development. Thus, the disruption of CS enables PP-m/PE-m1 to stretch more than the other two blends.

The PP phase in PP-m/PE-m1 50/50 blends forms a continuous phase and it should undergo shear yielding in the yielding region of Figure 1. The macroscopic behavior such as brittle-to-ductile transition indicates that the shear yielding in PP-m/PE-m1 50/50 blends is significantly promoted. Significant shear yielding can also cause the disruption process of the initiated

CS, resulting in higher strain-to-break. Thus, the uniqueness in the mechanical behavior of PP-m/PE-m1 50/50 blends relies on two factors, promoted shear yielding and disruption of CS into discrete nanopores. They might be closely related with each other.

The disruption process can occur when the initiation of CS is favorable and its further growth is prevented. The initiation of CS mainly depends on the level of triaxial stress, while shear yielding depends on the level of the von Mises stress component.[39–41] Once CS is initiated and starts to grow, the triaxial stress built up around it can be reduced.[39–41] Therefore, after the initiation of CS, shear yielding can be promoted and the further growth of crazes can be suppressed.

The stress concentration of von Mises and triaxial components depends on the modulus mismatch, morphology, and interfacial strength of two phases in binary blends. Modulus mismatch can be an important factor promoting shear yielding. Figure 1 shows that PE-m1 is considerably softer than PE-m2, resulting in the highest modulus mismatch in PP-m/PE-m1 50/50 blends. So, the von Mises stress component is the highest at the interface of the blends, if all other factors are the same. Since shear yielding depends on the von Mises stress component, the promotion of shear yielding can be expected in PP-m/PE-m1. However, this series of events might not be the major contribution, because the difference between the moduli of PP-m and PP-z does not seem to be significant. Thus, the difference between the mechanical behaviors of PP-m/PE-m1 and PP-z/PE-m1 cannot be explained using this modulus mismatch argument.

Morphological change is distinct in the blends because they undergo a phase inversion near 50/50 composition. The brittle-to-ductile transition occurs mainly because of the phase inversion. However, the brittle-to-ductile transition in Figure 2 does not exactly reflect the differences in morphology. To further explore the effect of morphology, the polyolefin systems will be studied with controlling their morphology (i.e., layered films) in a separate report. Interfacial strength will be further discussed as well.

CONCLUSION

The development of porous structures during the stretching of polyolefin films has been studied. The films have two types of polyolefins (one produced by metallocene and the other by Ziegler-Natta catalysts) mixed at a weight ratio near 50/50. PP-m/PE-m1 blends (metallocene pair) have longer strain-to-break values than the other blend systems. PP-m phase in the blend was continuous, but did not show its intrinsic brittle failure behavior. In the blend system, CS formation, shear yielding, and discrete nanopores were observed. Electron microscopy data reveal that the nanopores partially retain band-like structures, so they seem to result from the disruption of CS. As strain increases, CS becomes disrupted and develops into discrete nanopores instead of critical cracks. The disruption process seems to be important in stabilizing pore development. Differences in interfacial strength and phase structure could also contribute to the differences in strain-to-break. Simple stretching of this blend at room temperature can produce stable CS pores of 10–300 nm on and beneath the surface of films. It is feasible to control the pore morphology of films by changing strain rate or multiaxial stretching.

This study was funded by ExxonMobil Co. The authors thank Dr. Pat Brant of ExxonMobil for helpful discussion and Dr. David Bell of University of Minnesota for TEM training.

References

1. Druin, M. L.; Loft, J. T.; Plovan, S. G. U. S. Patent 3 801 404, 1974.
2. Kamada, K.; Minami, S.; Toshida, K. U. S. Patent 4 055 696, 1977.
3. Nago, S.; Mizutani, Y. J Appl Polym Sci 1998, 68, 1543.
4. Hedrick, J. L.; Carter, K. R.; Labadie, J. W.; Miller, R. D.; Volksen, W.; Hawker, C. J.; Yoon, D. Y.; Russell, T. P.; McGrath, J. E.; Briber, R. M. Prog Polyimide Chem 1999, 140, 1.
5. Gu, B.; Du, Q.; Yang, Y. J Membr Sci 2000, 164, 59.
6. Colvin, R. Modern Plastics 2000, June, 24.
7. Mizutani, Y.; Nago, S. J Appl Polym Sci 1999, 72, 1489.
8. Chaffin, K. A. Ph. D. Thesis. University of Minnesota, Twin Cities, 1999.
9. Chen, Y. Y.; Lodge, T. P.; Bates, F. S. J Polym Sci B, Polym Phys 2000, 38, 2965.
10. Chaffin, K. A.; Knutsen, J. S.; Brant, P.; Bates, F. S. Science 2000, 288, 2187.
11. Chaffin, K. A.; Bates, F. S.; Brant, P.; Brown, G. J Polym Sci B, Poly Phys 2000, 38, 108.
12. Yamaguchi, M.; Miyata, H. Macromolecules 1999, 32, 5911.
13. Wignall, G. D.; Alamo, R. G.; Londono, J. D.; Mandelkern, L.; Kim, M. H.; Lin, J. S.; Brown, G. M. Macromolecules 2000, 33, 551.
14. Dharmarajan, N. R.;Yu, T. C. Plastics Eng 1996, August, 33.
15. Deng, M.; Shalaby, S. W. Biomaterials 1997, 18, 645.
16. Lewis, G. Biomaterials 2001, 22, 371.
17. Karger-Kocsis, J. Macromol Symp 1999, 143, 185.
18. Trent, J. S.; Scheinbeim, J. I.; Couchman, P. R. Macromolecules 1983, 16, 589.
19. Montenzinos, D.; Wells, B. G.; Burns, J. L. J Polym Sci, Polym Lett 1985, 23, 421.
20. Sano, H.; Usami, T.; Nakagawa, H. Polymer 1986, 27, 1497.
21. Brown, G. M.; Butler, J. H. Polymer 1997, 38, 3937.
22. Qureshi, N. Z.; Rogunova, M.; Stepanov, E. V.; Capaccio, G.; Hiltner, A.; Baer, E. Macromolecules 2001, 34, 3007.
23. Willemse, R. C.; Speijer, A.; Langeraar, A. E.; Posthuma de Boer, A. Polymer 1999, 40, 6645.
24. Kausch, H.-H., Ed.; *Crazing in Polymers*; Adv Polym Sci 91/92; Springer-Verlag: New York, 1990.
25. Michler, G. H. Makromol Chem Macromol Symp 1991, 41, 39.
26. Starke, J. U.; Michler, G. H.; Grellmann, W. Seidler, S.; Gahleitner, M.; Fiebig, J.; Nezbedova, E. Polymer 1998, 39, 75.
27. Weidisch, R.; Horig, E.; Lach, R.; Enblen, M.; Micher, G. H.; Stamm, M.; Jerome, R. Polym Adv Technol 1998, 9, 727.

28. Lin, C. H.; Yang, A. C.-M. J Mater Sci 2000, 35, 4231.
29. Krupenkin, T. N.; Fredrickson, G. H. Macromolecules 1999, 32, 5029.
30. Krupenkin, T. N.; Fredrickson, G. H. Macromolecules 1999, 32, 5036.
31. Hristov, H. A.; Yee, A. F.; Xie, L.; Gidley, D. W. Polymer 1994, 35, 4287.
32. Morelli, T. A.; Takemori, M. T. J Mater Sci 1984, 19, 385.
33. Manaure, A. C.; Muller, A. J. Macromol Chem Phys 2000, 201, 958.
34. Laurens, C.; Ober, R.; Creton, C.; Léger, L. Macromolecules 2001, 34, 2932.
35. Shanks, R. A.; Li, J.; Yu, L. Polymer 2000, 41, 2133.
36. Nago, S.; Mizutani, Y. J Appl Polym Sci 1996, 61, 31.
37. Chu, F.; Kimura, Y. Polymer 1996, 37, 573.
38. Mark, J. E.; Eisenberg, A.; Graessley, W. W.; Mandelkern, L.; Samulski, E. T.; Koenig, J. L.; Wignall, G. D. Physical Properties of Polymers, 2nd ed.; Cambridge University Press: Cambridge, UK, 1993.
39. Kinloch, A. J.; Young, R. J. *Fracture Behavior of Polymers*, Amsterdam: Elsevier, 1985.
40. Yee, A. F.; Pearson, R. A. J Mater Sci 1986, 21, 2462.
41. Lee, J.; Yee, A. F. Polymer 2001, 42, 577.